# Chemisorption of Hydroxide on 2D Materials from DFT Calculations: Graphene versus Hexagonal Boron Nitride

Benoit Grosjean,[†] Clarisse Pean,[†] Alessandro Siria,[‡] Lydéric Bocquet,[‡] Rodolphe Vuilleumier,[†] and Marie-Laure Bocquet*,[†]

[†]École Normale Supérieure-PSL Research University, Département de Chimie, Sorbonne Universités - UPMC Univ Paris 06, CNRS UMR 8640 PASTEUR, 24, rue Lhomond, 75005 Paris, France

[‡]École Normale Supérieure-PSL Research University, Laboratoire de Physique Statistique, UMR 8550, 24, rue Lhomond, 75005 Paris, France

S *Supporting Information*

ABSTRACT: Recent nanofluidic experiments revealed strongly different surface charge measurements for boron-nitride (BN) and graphitic nanotubes when in contact with saline and alkaline water (*Nature* **2013**, *494*, 455−458; *Phys. Rev. Lett.* **2016**, *116*, 154501). These observations contrast with the similar reactivity of a graphene layer and its BN counterpart, using density functional theory (DFT) framework, for intact and dissociative adsorption of gaseous water molecules. Here we investigate, by DFT in implicit water, single and multiple adsorption of anionic hydroxide on single layers. A differential adsorption strength is found in vacuum for the first ionic adsorption on the two materials—chemisorbed on BN while physisorbed on graphene. The effect of implicit solvation reduces all adsorption values, resulting in a favorable (nonfavorable) adsorption on BN (graphene). We also calculate a $pK_a \simeq 6$ for BN in water, in good agreement with experiments. Comparatively, the unfavorable results for graphene in water echo the weaker surface charge measurements but point to an alternative scenario.
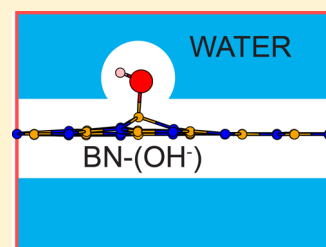
The successful isolation of single-layer graphene sheet[3] has led to tremendous progress in the discovery of new 2D materials including boron nitride (BN), silicene, and transition-metal dichalcogenides to cite a few. In particular, hexagonal BN monolayers share the planar honeycomb structure of graphene, with boron and nitrogen atoms alternating in the vortices of the honeycomb structure. Despite their similar crystallographic structure, the electronic structures of BN and graphene nanosheets are drastically different: semimetallic for graphene and insulating for BN. Until recently, both pristine layered materials were assumed to present inherently low chemical reactivity. However, recent experimental works showed that covalent chemical functionalization could be achieved under drastic reactive conditions, either via reduction[4,5] or reaction with oxidative reagents (H_2O_2,[6] oxygen radical[7]) or via fluorination.[8] Furthermore, recent nanofluidic experiments have altered the long-standing picture of the chemical inertness of BN nanotubes by showing a large negative surface charge when the BN material is in contact with aqueous saline solutions. In contrast, similar experimental investigations based on nanofluidic investigations showed that carbon nanotubes[2] and planar graphitic surfaces[9] exhibit smaller and even minute surface charge.

The magnitude of the maximum charging, ranging from 0.1 C/m^2 for C to 1 C/m^2 for BN depending on the solution pH, rules out point defects as the sole origin of the measured surface charging. These experimental results therefore call for two challenging questions: (i) What are the potential chemical species present in basic and saline solutions that could adhere

on the surface and strongly charge the pristine nanotubes? (ii) How can we explain the different charging behavior of graphene and BN ideal nanotubes?

A recent DFT study has investigated the dissociation barrier of a water molecule in contact with pristine graphene and BN nanosheets and concluded that the process is highly endothermic with a larger barrier on graphene than on BN.[10] They also proposed facile ways to enhance the dissociation, either via including substitutional defects or via preadsorption of H, which again amounts to the presence of defects.

Here in this DFT work we consider pristine nanosheets and take into account the presence of hydroxide ions in water. We demonstrate that adding one electron (via the charged adsorbate) to these 2D materials permits us to tune the adsorption strength of one hydroxide: a strong ionic adsorption on BN and a weak ionic adsorption on graphene. Our atomistic results corroborate the acidity (pK_a) of the BN sheet, pointing to the hydroxide anion as the best candidate to explain the charging of BN material immersed in a saline electrolyte.

The total energies of the systems have been calculated using the periodic DFT code Vienna Ab initio Simulation Package (VASP) (see Methods). The graphene and h-BN single layers were modeled using the same supercell corresponding to an (3 × 5) orthorhombic unit cell containing 60 atoms under periodic boundary conditions (PBCs) (see Figure 1). The slab
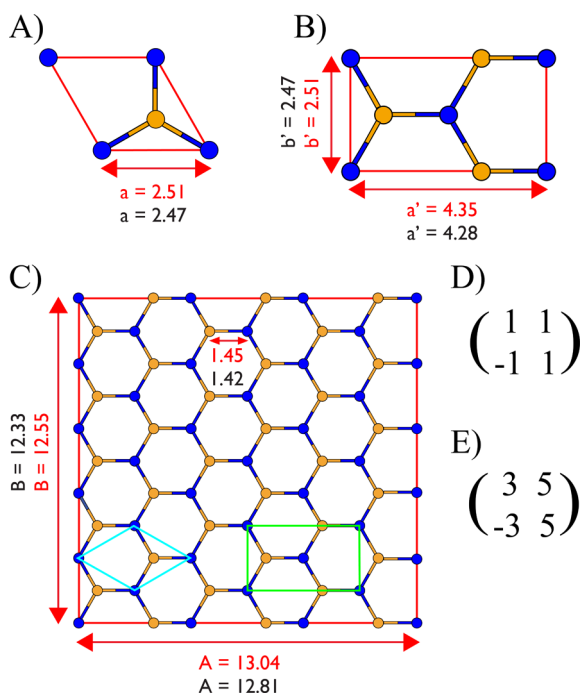
Figure 1. (A) BN hexagonal primitive unit cell. (B) BN orthorhombic primitive unit cell. (C) BN orthorhombic supercell adopted in the DFT calculations. Distances, expressed in angstroms, are written in red (black) for the case of BN (graphene). Boron, carbon, nitrogen, oxygen, and hydrogen are respectively displayed in yellow, gray, blue, red, and pink. (D) Matrix to transform cell (A) into cell (B). (E) Matrix to obtain cell (C) from cell (A).
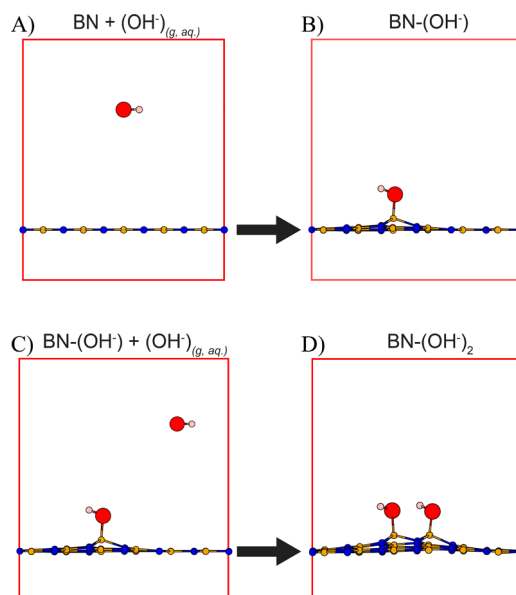

Figure 2. (top) Simulation cells for the BN monolayer (same on graphene not shown) used to determine the energy of the adsorption of the first anionic hydroxide. (A) Sub + OH_f: substrate and one desorbed anionic hydroxide in gaseous or aqueous phase. (B) OH_a: substrate with an adsorbed hydroxide onto either a B atom (BN layer) or a C atom (graphene layer). (bottom) Simulation scheme used to determine the energy of the adsorption of a second hydroxide. (C) $OH_a + OH_f$: a surface with an adsorbed hydroxide and a desorbed hydroxide in gaseous or aqueous phase. (D) 2 OH_a: a substrate with two adsorbed hydroxides. See Figure 1 caption for color code of the atoms.

monolayer is separated by a vacuum space of 15 Å to avoid the interaction between the periodic images. The gamma point has been used in the k-point sampling of the first Brillouin zone of the supercell. The graphene and h-BN bond distances are evaluated to 1.43 and 1.45 Å with the Perdew, Burke, and Ernzerhof (PBE) functional, in agreement with previous calculations with the same method.[11] We study the adsorption of anionic hydroxide molecule onto one B (or C) atom of the sp^2 BN (graphene) layer, respectively. The resulting adsorption state is therefore negatively charged, and a homogeneous background charge is automatically added in the periodic supercell to ensure its neutrality. As a result, the total energy of a charged solid system includes an additional electrostatic interaction with the charged background. To compute the first adsorption energy of OH^- called E_{ads1}, we consider the adsorbed OH on a negatively charged surface (by adding an extra electron to the total valence electrons) as the final state and the noninteracting species taken in the same supercell as the initial state, as shown in Figure 2A,B. By doing so, the additional electrostatic interaction with the charged vacuum cancels out in the resulting adsorption energy.

$$E_{ads1} = E(OH_a) - E(OH_f) \qquad (1)$$

where the indices a and f stand for adsorbed and desorbed OH^- respectively (see Figure 2 caption). The second adsorption energy proceeds similarly as illustrated in Figure 2C,D.

$$E_{ads2} = E(2OH_a) - E(OH_a + OH_f) \qquad (2)$$

Table 1 summarizes the energetics computed within periodic DFT for the first OH^- adsorption on pristine BN and graphene monolayers subjected to different environments. In vacuum, the

Table 1. Adsorption Energies (in eV) of the First OH^- Species onto BN and Graphene Layers in Vacuum and in Implicit Water[a]

OH^- ($OH\cdot$)	BN layer	graphene layer
E_{ads1}	−2.3 (−0.63, M = 1)	−0.5 (−0.57, M = 1)
E_{ads1}^{sol}	−0.89	+0.33
$E_{ads1}(vdw)$	−2.1	−0.52
$E_{ads1}^{sol}(vdw)$	−0.9	+.33

[a]Negative (positive) values mean favorable (unfavorable) cases. For the adsorption in vacuum, values in parentheses are spin-polarized calculations for the uncharged system, that is, the radical $OH\cdot$ adsorption that induces magnetism in graphene with M the electron magnetism.

adsorption is strongly favorable with −2.3 eV on BN layer, while it is less favored on the graphene layer (−0.5 eV). The obtained values are strikingly different for both materials. The difference can be assigned to the charged ligand. Comparatively the neutral adsorption computed with spin-polarized calculations leads to similar moderate values (around −0.6 eV), in full agreement with previous studies.[10,12] Interestingly the adsorption values do not depend on the inclusion, or not, of van der Waals (vdw) corrections (see $E_{ads1}(vdw)$ in Table 1). Indeed, in the final adsorption state the species are short-range bonded precluding vdw interactions, and in the initial desorbed state the species are positioned to avoid any spurious vdw interaction.

In contrast, the adsorption values in implicit water are greatly reduced by ~1 eV, maintaining a favorable adsorption value for BN while turning to an unfavorable adsorption value for

graphene. Notably, including the solvent in the DFT modeling permits us to discriminate both materials regarding the adsorption of one anionic hydroxyl: BN will spontaneously attach, while graphene should remain inert at least at low temperatures. We note in passing an alternative way to model the adsorption of a charged ligand with zero net charge in the supercell: the insertion of a counterion such as one potassium cation in the vacuum space at long distance from the adsorbate and the surface. The resulting energetics including the potassium cation are very similar to the charged procedure used in this study (see Supporting Information). Hence the discriminative energetics between the two materials are robust against different modeling schemes of the charging effect.

The detailed DFT geometries of the adsorbed structures are displayed in Figure 3. Side views permit us to visualize the sp^3
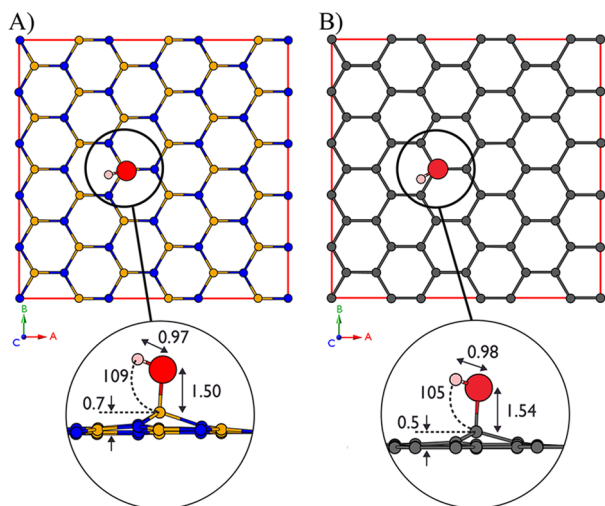

Figure 3. DFT adsorption structures. Top views of BN (A) and graphene (B). Insets with side views of the bonding site for each material with key distances and angles expressed in angstroms and degrees, respectively. See Figure 1 caption for color code of the atoms.

rehybridization of the bonding atom inducing an out-of-plane buckling somewhat larger for BN than for graphene. The bonding distances between the O atom and the anchoring site on the substrates are 1.5 Å for BN and 1.54 Å for graphene, typical for single C−O bonds. A pyramidalization angle θ_p[13] can be determined and amounts to 18° for BN and 15° for graphene corresponding to 93 and 77% of sp^3 hybridization, respectively. The geometrical differences are not as striking as the energy differences, but it confirms a weaker adsorption of OH⁻ on graphene than on BN.

We have investigated the spatial distribution of the additional electron using the Mulliken charge analysis (see Methods). It strongly differs between BN and graphene nanosheets (see Supplementary Table). The grafted C atom on graphene gains only 0.06 electron, and the rest of the C atoms remain practically noncharged. On graphene the additional charge is totally delocalized over the nanosheet, and the possible charge-activating role to bind hydroxyl is therefore masked. In contrast, on BN the grafted B gains 0.22 electron and becomes less positively charged than the rest of electron-deficient B atoms. The additional charge on BN is therefore substantially localized on the ligand, and the grafted atom and the local reduction of the binding B atom can explain its improved reactivity.

We then studied the adsorption of a second OH⁻ ion onto BN and graphene monolayers. Figure 4 displays the second
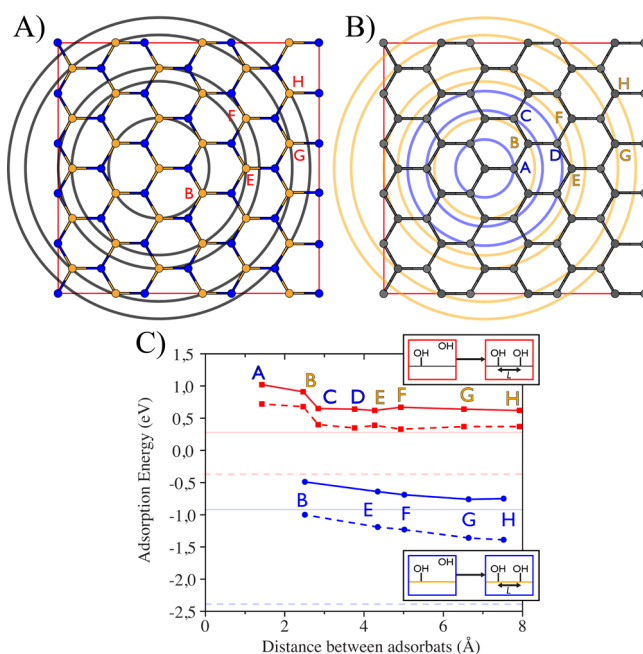

Figure 4. (A) Circles display possible sites (labeled with letters) for the second adsorption of OH⁻ at a given distance from the first adsorption site labeled A. (B) Same for graphene. (C) Adsorption energy of a second hydroxide versus the distance between the two adsorption sites. Results for BN are displayed by circles connected by blue lines while results for graphene are represented by squares connected by red lines. Horizontal lines represent the adsorption energies for single OH⁻ ions (blue for BN, red for graphene). Plain and dashed lines, respectively, correspond to adsorptions in implicit water and in vacuum. See Figure 1 caption for color code of the atoms.

adsorption energy in vacuum E_{ads2} (dashed lines) and in implicit solvent E_{ads2}^{sol} (solid lines) as a function of the distance L from the first adsorption site. Circles mark the successive next-nearest neighbors. Because only every two atoms are available for OH⁻ adsorption on h-BN, there are two times more such sites on graphene as compared with BN.

As shown on Figure 4, the addition of a second OH⁻ ion on the nearest neighbor located in the same hexagon destabilizes the adsorption energy by typically ∼1 eV, as compared with the single ion adsorption. It remains favorable for BN (point B) but becomes readily unfavorable for graphene (point A).

The second adsorption energy is then found to decrease as a function of the distance L from the first ion. The value reaches a plateau in energy for large values of L, slightly above the first adsorption value. Typically the plateau is reached roughly beyond $L = 3$ Å for graphene and beyond $L = 5$ Å for BN. Now considering the effect of the solvent, one may observe that it leads to a global destabilizing shift for the second adsorption energy, typically ∼0.3 to 0.5 eV. The difference in energy between the first adsorption and the plateau is, however, reduced as compared with vacuum. One may attribute this effect to the screening of charge.

In the following we compute the thermodynamics of adsorption of OH⁻ on the BN or graphene layers following successful approaches adapted to solid interfaces[14−16] (see the Supporting Information). The correction terms that link E_{ads1}^{sol} to the Gibbs free energy of first adsorption ΔG_{ads1} were

evaluated at $T = 293.15$ K and considering a solute standard concentration $c^0 = 1$ mol L^{-1}. The thermodynamic corrections are summarized in Table 2, while more details are available in

Table 2. Thermodynamic Corrections and the Gibbs Free Energy of the First Adsorption Evaluated in eV at 297.15 K and 1 bar[a]

OH$^-$	BN layer	graphene layer
T (K)	297.15	
ϵ_b ($P = 1$ bar)	78.4	
E_{ads1}^{sol}	−0.89	+0.33
correction	+0.43	+0.46
$\Delta G_{ads1}(T, P)$	−0.46	+0.79

[a] ϵ_b designates the dielectric permittivity of the solvent. All energies are expressed in electronvolts.

the Supporting Information. As a result, we find a favorable $\Delta G_{ads1} = -0.46$ eV for BN and a nonfavorable $\Delta G_{ads1} = +0.79$ eV for graphene. Thermodynamic corrections also worsen the scenario for the graphene material. This result rules out this charging mechanism on bare graphene but permits us to envision it for BN.

We further quantified how the predicted adsorption energies ΔG_{ads1} compare with the surface charge data extracted from the BN measurements in ref 1. From the value of ΔG_{ads1}, one can define the surface pK_a as

$$\mathrm{p}K_a = 14 + \frac{\Delta G_{ads1}}{k_B T \times \log(10)} \tag{3}$$

As an overall result, eq 15 predicts p$K_a = 6$ for BN and p$K_a = 27.7$ for graphene. The value for BN agrees well with the post-treatment of experimental data,[1] in which the electrostatic potential at the surface was evaluated using the Poisson–Boltzmann model. The value proposed for graphene is nonrealistic precluding the same mechanism on graphene.

Our results support the strong reactivity of BN monolayer in the presence of hydroxyl anions contained in saline water. The contrasted result on graphene confirms the differential chemical behavior between the two materials. This echoes the experimental results using nanofluidic tools where much smaller adsorption is found on carbon nanotubes and planar graphitic surface.[2,9] Still the presence of a surface charge on carbon tubes may suggest that other species than OH$^-$ could adsorb onto the graphene surface and charge it.

Another interesting parameter is the maximum coverage for the ions on the surface. Such a quantity enters the global thermodynamics when considering for example the charge–pH relationship in the experiments. The adsorption equilibrium

$$\mathrm{Sub} + \mathrm{OH}_{aq}^- \Leftrightarrow \mathrm{Sub} - \mathrm{OH}_{ads}^- \tag{4}$$

is usually modeled by a Langmuir adsorption model, which introduces a maximal fraction $\theta_{max} < 1$ of B or C atoms (for h-BN or graphene, respectively) that constitute possible adsorption sites. This value for θ_{max} fixes the maximal charge expected on the surface, which is an interesting quantity per se. Denoting θ the fraction of bonded B or C atoms to an adsorbed OH$^-$, the chemical potential of OH$^-$ at the surface is then modeled as

$$\mu_s = \Delta G_{ads1} - e\phi + k_B T \log\left(\frac{\theta}{\theta_{max} - \theta}\right) \tag{5}$$

where ϕ is the electrostatic potential at the surface. The chemical potential of OH$^-$ in the bulk at the concentration [OH$^-$] expressed in mol L^{-1} is fixed at equilibrium by its bulk value.

$$\mu_b = k_B T \log[\mathrm{OH}^-] \tag{6}$$

so that

$$\frac{\Delta G_{ads1}}{k_B T} - \frac{e\phi}{k_B T} + \log\left(\frac{\theta}{\theta_{max} - \theta}\right) = \log[\mathrm{OH}^-] \tag{7}$$

The equilibrium condition then becomes

$$\log\left(\frac{\theta}{\theta_{max} - \theta}\right) = \frac{e\phi}{k_B T} + \log(10)(\mathrm{pH} - \mathrm{p}K_a) \tag{8}$$

which relates the surface coverage to pH of the solution and the electrostatic potential at the surface.

A rough estimate for θ_{max} can be done for BN on the basis of our DFT calculations. To this aim, we performed preliminary investigations of further adsorption of hydroxyl anions keeping the same minimum favorable distance revealed in Figure 4. First results are presented in Figure 5. Considering a third adsorption on the same hexagon leads to an energetically unfavorable configuration (plot B). The adsorption of three adsorbates in a raw is energetically favorable, although the zigzag configuration (plot C) is less favorable than the straight
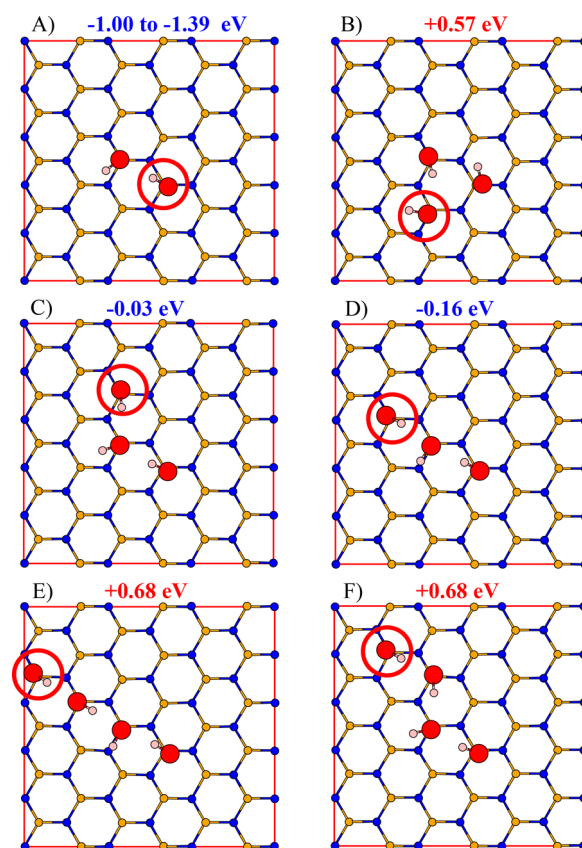

Figure 5. Beyond the second adsorption on BN monolayer: from two adsorbates in the same honeycomb at the minimum favorable distance (A) exploration of three adsorbates (B−C−D) and four adsorbates (E−D) keeping the same favorable distance. The indicated energy is the adsorption energy of the last adsorbate which is identified by a red circle. See Figure 1 caption for color code of the atoms.

segment (plot D). Finally, completing the lines with a fourth adsorbate becomes nonfavorable (plots E and F). Of course these are first configurations, and the stability of many other configurations should be evaluated. This goes beyond the present work and will be the object of a forthcoming study. However, on the basis of these results, one may estimate that three hydroxides can be grafted at most in a rectangle of $(L + l_{3OH}) \times L$, which amounts to a surface of 50 Å^2, with l_{3OH} the distance between 3 hydroxides adsorbed in a line pattern (see Figure 5D). This corresponds to a site density of 0.06 per Å^2, and the associated full-coverage site density is ~0.18 per Å^2 (30 B atoms per supercell). This leads to $\theta_{max} \simeq 0.33$ and $\Sigma_{max} \simeq 0.96$ Cm^{-2}. These values are in good agreement with the values reported for the maximum charge measured on BN surfaces.[1]

In conclusion, we have investigated comparatively within ab initio DFT framework a monolayer of BN and graphene embedded in implicit water and in contact with one hydroxyl anion. We predict for the first time a contrasted chemical reactivity for graphene and BN: a chemisorption of OH$^-$ on BN, while this mechanism is not highlighted on graphene. This striking difference between the two pristine materials is linked to their electronic structure and the lack of screening for graphene surface as compared with the insulating BN. Furthermore, on the basis of atomistic thermodynamics including all of the vibrational contributions to energy and entropy, we have derived a free energy of adsorption of −0.46 eV on BN, which corresponds to a p$K_a \simeq 6$, in quantitative agreement with experimental measurements.[1] Hence this charging scenario is viable on BN, and our study leans strong support to the recently revealed noninertness of the BN material in contact with aqueous saline phase. On the contrary, the case of graphene requires further investigations. Indeed, planar graphitic surfaces show minute surface charge (as deduced from surface conductance measurements),[9] while the experiments on carbon nanotubes still exhibit a surface charge,[2] although much weaker as compared with BN tubes.[1] This suggests the possibility of adsorption of other charged species on the carbon surfaces, not considered in the present study. Future work will involve the exploration at finite T of the charging mechanism using explicit water solvent and the inclusion of counterions using ab initio molecular dynamics (AIMD) to evaluate a more realistic pK_a value. Also, taking the full stacking of these 2D materials into account, their curvature effect (since the measurements are made on multiwall nanotubes of different lengths and diameters) is another ingredient that will be of high interest in understanding the molecular mechanisms at stake in the chemical reactivity of these 2D materials.

METHODS

Ab Initio Calculations. Using the VASP code,[17−19] the wave functions of the system contained in the supercell have been expanded in a plane-wave basis set with an energy cutoff of 800 eV. The common cutoff for hybrid interfaces is 400 eV in vacuum, and taking twice the value is requested for the sake of precision when dealing with the implicit solvent scheme (see below). The electronic cores are described by the projector augmented wave method.[20] The exchange-correlation energies have been evaluated within the generalized gradient approximation (GGA).We employ GGA functionals as suggested by Perdew, Burke, and Ernzerhof (PBE).[21,22] However, we have also verified that the key results (adsorption energies) obtained here are not particularly sensitive to the choice of exchange-

correlation functional, in particular, using the vdW-inclusive optB86b-vdW functional[23,24] that includes vdw interactions. We use the smearing technique using a Gaussian broadening of 0.2 eV to achieve electronic convergence. To check the possible influence of the calculation settings, we have modified sequentially the smearing value to 0.1 eV, the k-mesh to 3 × 3 × 1, and the vacuum space to 20 Å. The adsorption values vary between 0.1 and 0.2 eV, but the striking difference between graphene and BN adsorption energies holds true.

In a second step the solvation energies in implicit water (E^{sol}) are evaluated within the joint density functional theory framework, as implemented into VASP by Mathew and Hennig[25] and successfully used recently.[26−29] In this technique the dielectric permittivity of the medium is defined as a functional of the electronic density. Indeed, dielectric permittivity asymptotically approaches the bulk water value at 1 bar, $\epsilon_b = 78.4$, in the region where the electronic density is lower than $\rho_{cut} = 0.0025$ Å^3 (the default cutoff charge density), while $\epsilon_b = 1$ in the region where the electronic density is high (inside the slab treated as a solute). The cavitation energies that account for the solvent contributions are calculated with a surface tension parameter of 0.525 meV/Å^2. The systems are fully optimized in vacuum with atomic forces lower than 0.02 eV/Å. Then, the optimized vacuo geometries are subjected to the implicit solvent interaction and the total energies named E^{sol} are corrected after an energy and geometry optimization. For the second adsorption, E_{ads2}, however we use the frozen geometry from vacuum for the sake of computational time. As a result, the adsorption energy in implicit water transforms into

$$E_{ads1}^{sol} = E^{sol}(OH_a) - E^{sol}(Sub + OH_f) \tag{9}$$

To evaluate the vibrational entropic corrections to this adsorption energy, we have run a vibrational analysis of states A and B (see Figure 2) to determine the vibrational modes and frequencies. The classical procedure in VASP is to calculate and diagonalize the Hessian matrix using the finite-difference method.

In addition, we derived Mulliken atomic charges from a static Dmol3 calculation[30−32] based on the VASP-optimized structures to understand the spatial location of the excess charge.

■ ASSOCIATED CONTENT

Ⓢ Supporting Information

The Supporting Information is available free of charge on the ACS Publications website at DOI: 10.1021/acs.jpclett.6b02248.

> Table 1: Adsorption energy of a hydroxide on BN and graphene layers in vacuum and in implicit water with and without a potassium counterion present in the supercell. Table 2: Mulliken atomic charges expressed in elemental charge. Table 3: Detailed thermodynamic corrections and the Gibbs free energy of the first adsorption evaluated in eV at 297.15 K and 1 bar. (PDF)

■ AUTHOR INFORMATION

Corresponding Author

*E-mail: marie-laure.bocquet@ens.fr.

ORCID Ⓞ

Marie-Laure Bocquet: 0000-0001-7122-4907

Notes

The authors declare no competing financial interest.

ACKNOWLEDGMENTS

REFERENCES

(1) Siria, A.; Poncharal, P.; Biance, A.-L.; Fulcrand, R.; Blase, X.; Purcell, S. T.; Bocquet, L. Giant Osmotic Energy Conversion Measured in a Single Transmembrane Boron Nitride Nanotube. *Nature* **2013**, *494*, 455−458.

(2) Secchi, E.; Niguès, A.; Jubin, L.; Siria, A.; Bocquet, L. Scaling Behavior for Ionic Transport and its Fluctuations in Individual Carbon Nanotubes. *Phys. Rev. Lett.* **2016**, *116*, 154501.

(3) Novoselov, K. S.; Geim, A. K.; Morozov, S. V.; Jiang, D.; Zhang, Y.; Dubonos, S. V.; Grigorieva, I. V.; Firsov, A. A. Electric Field Effect in Atomically Thin Carbon Films. *Science* **2004**, *306*, 666−669.

(4) Sun, Q.; Li, Z.; Searles, D. J.; Chen, Y.; Lu, G. M.; Du, A. Charge-Controlled Switchable CO_2 Capture on Boron Nitride Nanomaterials. *J. Am. Chem. Soc.* **2013**, *135*, 8246−8253.

(5) Shin, H.; Guan, J.; Zgierski, M. Z.; Kim, K. S.; Kingston, C. T.; Simard, B. Covalent Functionalization of Boron Nitride Nanotubes via Reduction Chemistry. *ACS Nano* **2015**, *9*, 12573−12582.

(6) Zhi, C.; Bando, Y.; Terao, T.; Tang, C.; Kuwahara, H.; Golberg, D. Chemically Activated Boron Nitride Nanotubes. *Chem. - Asian J.* **2009**, *4*, 1536−1540.

(7) Sainsbury, T.; Satti, A.; May, P.; Wang, Z.; McGovern, I.; Gunko, Y. K.; Coleman, J. Oxygen Radical Functionalization of Boron Nitride Nanosheets. *J. Am. Chem. Soc.* **2012**, *134*, 18758−18771.

(8) Tang, C.; Bando, Y.; Huang, Y.; Yue, S.; Gu, C.; Xu, F.; Golberg, D. Fluorination and Electrical Conductivity of BN Nanotubes. *J. Am. Chem. Soc.* **2005**, *127*, 6552−6553.

(9) Radha, B.; Esfandiar, A.; Wang, F. C.; Rooney, A. P.; Gopinadhan, K.; Keerthi, A.; Mishchenko, A.; Janardanan, A.; Blake, P.; Fumagalli, L.; et al. Molecular Transport Through Capillaries Made With Atomic-Scale Precision. *Nature* **2016**, *538*, 222−225.

(10) Al-Hamdani, Y. S.; Alfé, D.; von Lilienfeld, O. A.; Michaelides, A. Tuning Dissociation Using Isoelectronically Doped Graphene and Hexagonal Boron Nitride: Water and Other Small Molecules. *J. Chem. Phys.* **2016**, *144*, 154706.

(11) Graziano, G.; Klimeš, J.; Fernandez-Alonso, F.; Michaelides, A. Improved Description of Soft Layered Materials with Van der Waals Density Functional Theory. *J. Phys.: Condens. Matter* **2012**, *24*, 424216.

(12) Ghaderi, N.; Peressi, M. First-Principle Study of Hydroxyl Functional Groups on Pristine, Defected Graphene, and Graphene Epoxide. *J. Phys. Chem. C* **2010**, *114*, 21625−21630.

(13) Niyogi, S.; Hamon, M. A.; Hu, H.; Zhao, B.; Bhowmik, P.; Sen, R.; Itkis, M. E.; Haddon, R. C. Chemistry of Single-Walled Carbon Nanotubes. *Acc. Chem. Res.* **2002**, *35*, 1105−1113.

(14) Reuter, K.; Scheffler, M. Composition and Structure of the $RuO_2(110)$ Surface in an O_2 and CO Environment: Implications for the Catalytic Formation of CO_2. *Phys. Rev. B: Condens. Matter Mater. Phys.* **2003**, *68*, 045407.

(15) Loffreda, D. Theoretical Insight of Adsorption Thermodynamics of Multifunctional Molecules on Metal Surfaces. *Surf. Sci.* **2006**, *600*, 2103−2112.

(16) Hill, T. *An Introduction to Statistical Thermodynamics*; Addison-Wesley Series in Chemistry; Dover Publications, 1960.

(17) Kresse, G.; Hafner, J. Ab Initio Molecular Dynamics for Liquid Metals. *Phys. Rev. B: Condens. Matter Mater. Phys.* **1993**, *47*, 558−561.

(18) Kresse, G.; Furthmüller, J. Efficiency of *Ab-Initio* Total Energy Calculations for Metals and Semiconductors Using a Plane-Wave Basis Set. *Comput. Mater. Sci.* **1996**, *6*, 15−50.

(19) Kresse, G.; Furthmüller, J. Efficient Iterative Schemes for *Ab Initio* Total-Energy Calculations Using a Plane-Wave Basis Set. *Phys. Rev. B: Condens. Matter Mater. Phys.* **1996**, *54*, 11169−11186.

(20) Kresse, G.; Joubert, D. From Ultrasoft Pseudopotentials to the Projector Augmented-Wave Method. *Phys. Rev. B: Condens. Matter Mater. Phys.* **1999**, *59*, 1758−1775.

(21) Perdew, J. P.; Burke, K.; Ernzerhof, M. Generalized Gradient Approximation Made Simple. *Phys. Rev. Lett.* **1996**, *77*, 3865−3868.

(22) Ziesche, P.; Kurth, S.; Perdew, J. P. Density Functionals from LDA to GGA. *Comput. Mater. Sci.* **1998**, *11*, 122−127.

(23) Klimeš, J.; Bowler, D. R.; Michaelides, A. Van der Waals Density Functionals Applied to Solids. *Phys. Rev. B: Condens. Matter Mater. Phys.* **2011**, *83*, 195131.

(24) Klimeš, J.; Michaelides, A. Perspective: Advances and Challenges in Treating Van der Waals Dispersion Forces in Density Functional Theory. *J. Chem. Phys.* **2012**, *137*, 120901.

(25) Mathew, K.; Sundararaman, R.; Letchworth-Weaver, K.; Arias, T. A.; Hennig, R. G. Implicit Solvation Model for Density-Functional Study of Nanocrystal Surfaces and Reaction Pathways. *J. Chem. Phys.* **2014**, *140*, 084106.

(26) Lespes, N.; Filhol, J.-S. Using Implicit Solvent in *Ab Initio* Electrochemical Modeling: Investigating Li^+/Li Electrochemistry at a Li/Solvent Interface. *J. Chem. Theory Comput.* **2015**, *11*, 3375−3382.

(27) Sakong, S.; Naderian, M.; Mathew, K.; Hennig, R. G.; Groß, A. Density Functional Theory Study of the Electrochemical Interface Between a Pt Electrode and an Aqueous Electrolyte using an Implicit Solvent Method. *J. Chem. Phys.* **2015**, *142*, 234107.

(28) Steinmann, S. N.; Michel, C.; Schwiedernoch, R.; Filhol, J.-S.; Sautet, P. Modeling the $HCOOH/CO_2$ Electrocatalytic Reaction: When Details Are Key. *ChemPhysChem* **2015**, *16*, 2307−2311.

(29) Garcia-Ratés, M.; López, N. Multigrid-Based Methodology for Implicit Solvation Models in Periodic DFT. *J. Chem. Theory Comput.* **2016**, *12*, 1331−1341.

(30) Delley, B. An All-Electron Numerical Method for Solving the Local Density Functional for Polyatomic Molecules. *J. Chem. Phys.* **1990**, *92*, 508.

(31) Delley, B. From Molecules to Solids with the DMol³ Approach. *J. Chem. Phys.* **2000**, *113*, 7756.

(32) Delley, B. Fast Calculation of Electrostatics in Crystals and Large Molecules. *J. Phys. Chem.* **1996**, *100*, 6107−6110.